IEEE Industry Application Society Annual Meeting, Chicago, September 30 – October 5, 2001

# Design and Experiments of A Novel Axial Flux Circumferential Current Permanent Magnet (AFCC) Machine with Radial Airgap

Jian Luo
Member, IEEE
Eaton-Aerospace
Actuations and Controls
4520 Electronics Place
Los Angeles, CA 90039
USA
Tel: (818)-550-4282
Fax: (818)-550-6874
Email:
jianluo@eaton.com

Surong Huang
Department of Automation
Shanghai University
149 Yan-Chang Road
Shanghai, 200072,
P. R. China
Tel: 86-21-5403 0882
Email:
srhuang@yc.shu.edu.cn

Shaotang Chen
Senior Member, IEEE
Delphi Research Labs
30500 Mound Road
Warren, MI 48090
USA
Tel: (810)-323-5995
Fax: (810)-
Email:
shaotang.chen
@delphiauto.com

Thomas A. Lipo
Fellow, IEEE
Department of Electrical and
Computer Engineering
University of Wisconsin-Madison
1415 Engineering Dr.
Madison, WI 53706, USA
Tel: (608)-262-0287
Fax: (608)-262-1267
Email: lipo@engr.wisc.edu

***Abstract*-In this paper, an improvement to the axial flux, circumferential current (AFCC) machine is presented by introducing a radial airgap instead of an axial airgap. Sizing equations and three-dimensional finite element analyses are presented to predict the flux distribution, inductance, torque capability and other performances of this novel machine. Time-domain simulations are also performed to confirm the analysis and operation with a power converter. Design guidelines have been summarized for the quest for machine topologies with high power density or high torque capability. A prototype of the machine had been designed, built and tested with a closed-loop drive system based on DSP technology. The test results of the system are compared with the estimations. It is found that the machine offers larger torque capability in comparison with traditional commercial induction machines and brushless permanent magnet machines.**

## I. INTRODUCTION

The traditional design of AC electrical machines assumes sinusoidal voltage sources, resulting in consequent sinusoidal emf and sinusoidal currents in the machines. It was recognized in [1] and [2], however, that the emergence of power electronic converters has removed the need for such a concept or basis for machine design. In fact, an increasing number of researchers have addressed these non-traditional machines optimized for operating with power converters by using non-sinusoidal emf and current [3-5]. In [6], a novel AFCC machine topology with an axial airgap (see Fig. 1) was introduced to achieve a larger power density than conventional machines, while requiring a simplified converter topology.

In this paper, as an extended research, a further improved AFCC machine with a radial airgap (Fig. 2) is proposed. A comparison of the sizing equations of the two versions of AFCC machines, i.e. radial vs. axial airgap, is presented. More importantly, optimal selections of design parameters, such as the aspect ratio $K_L$ and inner/outer diameter ratio $\lambda$ are investigated for use as design guidelines. To verify the feasibility of the novel radial airgap configuration, a single–phase, 12-pole machine is designed based on these guidelines. A three-dimensional finite element analysis and time-domain simulations are used to facilitate the design and predict its performance. A prototype of the designed AFCC machine, together with a DSP based controller is then implemented in hardware. Experimental tests are performed and results are compared with the theoretical predictions. A comparison of the power density of the new machinewith those of other types of electric machines is also provided.

As shown in Fig. 1, axial flux circumferential current (AFCC) machines consist of three parts, a stator with iron poles and permanent magnets (PMs), a circumferential winding and a rotor with salient poles sitting on a center cylindrical portion. The main flux provided by two nearby PMs is concentrated in the stator pole and become axially oriented. This flux then passes across the air-gap, the rotor pole and the rotor cylinder to return to the adjacent stator pole. The winding is designed to link all of the main flux. The rotor poles on the two end-plates are shifted by one pole pitch.

With the realization of an initial smaller prototype [6], the principle of operation of the AFCC machine has already been demonstrated. Although the initial prototype appears to work well in the present topology, there has been some concern about the axial force between the rotor and stator through the axial airgap. The unbalanced force due to mechanical tolerances between the two airgaps may be sufficiently high to require special axial thrust bearings. Machines with radial airgap experience the same problem of unbalanced force. However, the conventional bearings can handle this very well. Moreover, the use of ferrite PM materials can reduce material cost. For these reasons, a new topology of AFCC with a radial airgap has been developed, which is shown on Fig. 2.

This project was jointly funded by Wisconsin Electric machine and Power Electronics Consortium (WEMPEC) and National Science Foundation of China (#59877014).

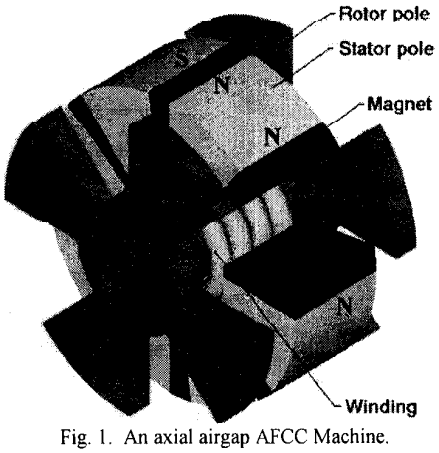


Fig. 1. An axial airgap AFCC Machine.

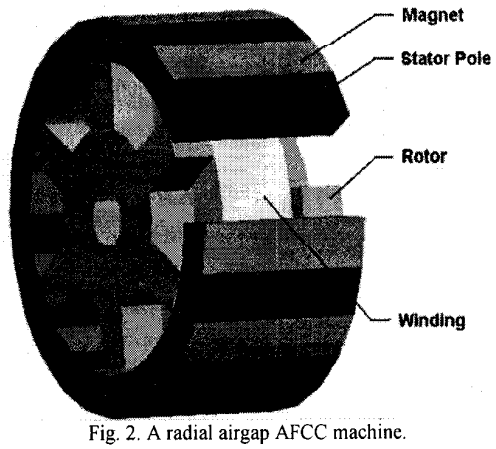


Fig. 2. A radial airgap AFCC machine.

## II. Sizing Equation Analysis

The approach for general-purpose sizing equations for conventional and unconventional machines has been developed in [2]. The sizing equation for the original axial-airgap AFCC machine has been given in [6] by exercising the general-purpose sizing equation, that is,

$$P_R(\text{Axial\_airgap}) = \frac{\pi}{2} pK_v K_m K_i K_p \eta B_g A \frac{f}{p}(1-\lambda^2) D_o^2 L_e \quad (1)$$

where

- $K_v$ Back emf wavform factor, or ratio of peak emf vs. average emf.
- $K_m$ The ratio of the area occupied by stator poles vs. the total area of stator airgap surface.
- $K_i$ current waveform factor.
- $K_p$ electrical power waveform factor.
- $\eta$ machine efficiency.
- $B_g$ flux density in the air gap.
- $A$ total electrical loading.
- $f$ converter frequency.
- $p$ machine pole pairs.
- $\lambda$ ratio of the diameter of the stator inner surface vs. that of the stator outer surface.
- $D_o$ diameter of the outer surface.
- $L_e$ effective stack length

Detailed explanations of these parameters can also be found in [2]. Following the same process as [6], the sizing equation for the novel radial-airgap AFCC machine is then derived as:

$$P_R(\text{Radial\_airgap}) = \pi pK_v K_m K_i K_p \eta B_g A \frac{f}{p} \lambda (1-\lambda) D_o^2 L_e \quad (2)$$

The power densities of the radial airgap AFCC machines and the axial airgap AFCC machines are then compared based on the same $\lambda$ and the same size.

$$\frac{P_R(Radial\_Airgap)}{P_R(Axial\_Airgap)} = \frac{\pi pK_m K_v K_i K_p \eta B_g A \frac{f}{p} \lambda(1-\lambda) D_o^2 L_e}{\frac{\pi}{2} pK_v K_m K_i K_p \eta B_g A \frac{f}{p}(1-\lambda^2) D_o^2 L_e} = \frac{2\lambda(1-\lambda)}{1-\lambda^2} = \frac{2\lambda}{1+\lambda} \quad (3)$$

The above ratio increases as $\lambda$ increases. For $\lambda = 0.85$, the above ratio is 0.92. In this case, the power density of the radial-airgap AFCC machines is slightly less (8%) than that of the axial-airgap machine, given that the other conditions are the same.

## III. Design and Modeling of the Prototype Motor

For the radial airgap AFCC machine (Fig. 2), the airgap flux density is given by

$$B_g = \frac{K_d(1-\lambda)D_o L_e B_u}{\frac{\pi\lambda D_o L_p K_m}{2p}} = \frac{K_d(1-\lambda)D_o L_e B_u}{\left(\frac{\pi\lambda D_o (1-\lambda) D_o K_m}{4p}\right)} = \frac{4pK_d B_u}{\pi K_m} \frac{L_e}{\lambda D_o} = \frac{4pK_d B_u}{\pi K_m} K_L \quad (4)$$

where $K_d$ is the airgap PM leakage factor, $L_p$ is the axial length of rotor pole, and $B_u$ is the residual flux density on the Surface of a permanent magnet (PM). Eq. (4) implies that, for an AFCC machine with a certain aspect ratio $K_L$, the airgap flux density will increase indefinitely as the pole number increases. However, the saturation of the material will limit this result. Hence, the selection of the aspect ratio $K_L$ should be related to the selection of the pole number. In a simple manner, if the pole number is doubled, the aspect ratio should become halved. As a result the larger the pole number is, the shorter the machine will become. It also appears that, in an AFCC machine with a given pole number, a larger the aspect ratio (longer machine) will result more flux to be concentrated to the airgap until the leakage

becomes the major factor to limit the airgap flux from increasing.

In PM machines, the windings normally do not link all of the flux of the PM material. The unlinked flux is considered as PM leakage. In AFCC machines, the PM leakage could be rather serious because of the three dimensional flux concentration structure. In order to indicate the leakage in the different sections of the machine, the airgap PM leakage factor $K_d$ can be defined as the ratio of the flux in the airgap over the total flux on the surface of the PM material. The total PM leakage factor $K_{do}$ is then defined as the flux in the rotor yoke linked by the winding over the total flux on the surface of the PM material. It is then necessary to determine these factors by three dimensional magnetic field analyses for the AFCC machines.

A series of models have been studied with the aid of Maxwell 3-D field analysis software. The flux on the surface of the PMs, the flux on the top of the rotor poles and the flux in the rotor yoke are calculated by integrating the flux densities on these surfaces. For example, in an AFCC machine with 12 poles, the flux densities on the surface of one of the PMs, on the top of one rotor pole and in the rotor yoke are shown in Fig. 3, Fig. 4 and Fig. 5 respectively. The leakage factors can be calculated from the field analysis results and they are then shown on Fig. 6. They can be used for selection of the aspect ratio $K_L$.

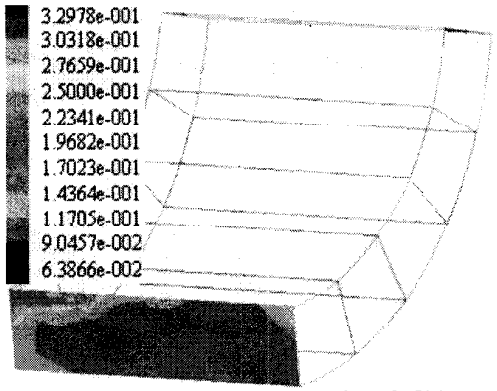


Fig. 3. Flux density on the surface of a PM.

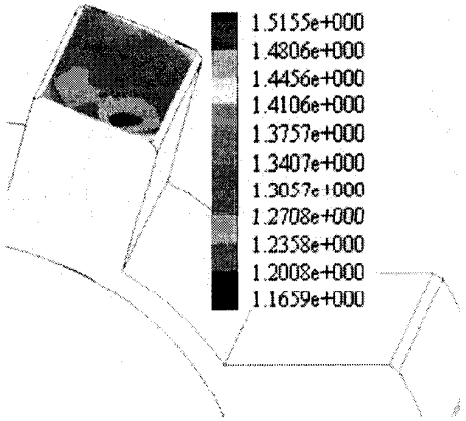


Fig. 4. Flux density on the top of a rotor pole.

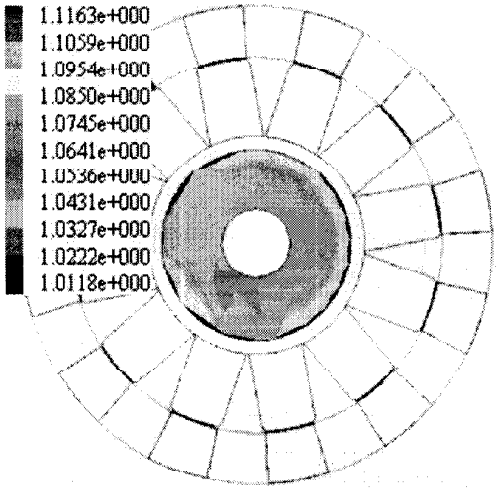


Fig. 5. Flux density in the rotor yoke.

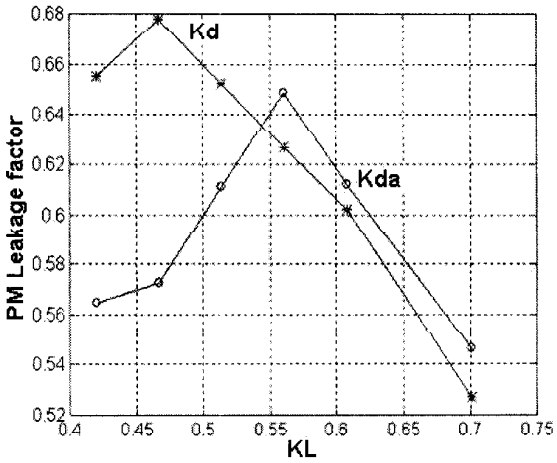


Fig. 6. PM leakage factor vs. aspect ratio $K_L$.

By examining the variation of PM leakage on Fig. 6, it is very interesting to find that $K_L$ = 0.54 is a distinguishing point. If $K_L$ is smaller, a part of airgap flux leaks back to stator before entering the rotor yoke. If $K_L$ is larger, a part of stator flux leaks to the rotor yoke without passing the airgap over the teeth. For an optimized design, it is suggested to select $K_L$ near to the value of 0.54 to form a balanced flux distribution.

Another important design factor is the parameter λ, which is defined as the ratio of the airgap diameter over the stator outer diameter. A cross section of the AFCC machine is shown on Fig. 7. Because the flux path needs to be balanced, the axial length of the rotor pole plate, $L_p$, should be equal to the radial thickness of the stator.

$$L_p = \frac{(1-\lambda)D_o}{2} \tag{5}$$

If λ increases, $L_p$ should decrease. The flux is reduced but more room needs be made available for the winding. Hence there must be an optimized value of λ for balanced distribution of iron and copper.

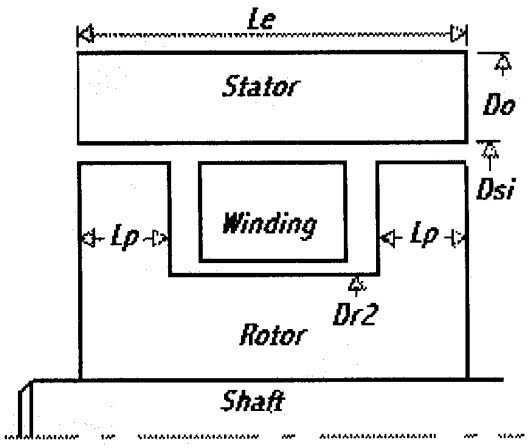

Fig. 7. The cross section of an AFCC machine

The sizing equation is then rewritten by introducing definition of electric loading $A$ for an AFCC machine [6].

$$P_R = \pi\, pK_m K_i K_p \eta\, B_g \frac{f}{p} D_o^{\,2}\, \lambda(1-\lambda)(AL_e)$$

$$= \pi\, pK_m K_i K_p \eta\, B_g \frac{f}{p} D_o^{\,2}\, \lambda(1-\lambda) N_t I_{rms} \qquad (6)$$

where $N_t$ is the number of turns of the winding and $I_{rms}$ is the rms current in the winding.

By definition [6], the total current in the winding is

$$N_t I_{rms} = J_s K_{cu} S_w \qquad (7)$$

where $J_s$ is the current density, $K_{cu}$ is the copper fill factor and $S_w$ is the cross section area of the winding, and

$$S_w = \frac{D_{si} - D_{r2}}{2}(L_e - 2L_p) \qquad (8)$$

Also due to the consideration of the balanced path of the flux, refer to Fig. 7, the diameter of the rotor yoke ($D_{r2}$) and the axial length of the rotor pole plate ($L_p$) should satisfy the equation:

$$\frac{\pi}{4}(D_{r2}^2 - D_s^2) = \frac{\pi D_{si} L_p K_m}{2} \qquad (9)$$

where $D_s$ is the diameter of the shaft, $p$ is the number of pole pairs and $D_{si}$ is the inner diameter of the stator ($D_{si}$= $\lambda D_o$). Referring to Eq. (5-3),

$$D_{r2} = \sqrt{\lambda(1-\lambda)D_o^2 K_m + D_s^2} \qquad (10)$$

Combining Eqs. (6) through (10), the relation between the rated power and the factor λ is determined as

$$P_R = \frac{p}{2}\pi K_m K_i K_p \eta\, B_g \frac{f}{p} D_o^2\, \lambda(1\text{-}\lambda) J_s K_{cu}$$

$$\bullet(\lambda D_o - \sqrt{\lambda(1-\lambda)D_o^2 K_m + D_s^2})(K_L \lambda D_o - (1-\lambda)D_o) \qquad (11)$$

In order to provide a numerical solution, it is suggested to assume some common values for those factors which are independent from parameter λ, such as

$p$ = 6, $K_m$ = 0.5, $K_i$ = 1.134, $K_p$ = 0.777, $K_v$ = 1.29,

$\eta$ = 0.80, $f$ = 75 Hz, $J_s$ = 6 A/mm$^2$ and $K_{cu}$ =0.32.

The variation rated power of the AFCC machines with different diameters and different λ can then be calculated by Eq. (6) and plotted on Fig. 8. It can be found that the optimal value of λ appears around λ=0.86, where the rated power reach their maximum values. Moreover, the optimal value of λ is independent from the size of the machines.

When selecting a proper λ for a machine, the electric loading should also be considered. The electric loading is shown on Fig. 9. For a small machine, a smaller electric loading should be selected considering the thermal conditions. Hence the suitable electric loading may be smaller that referred by an optimized λ of 0.85. In this case, the ratio λ should be selected smaller than the optimized value as a compromise to the limit of electric loading.

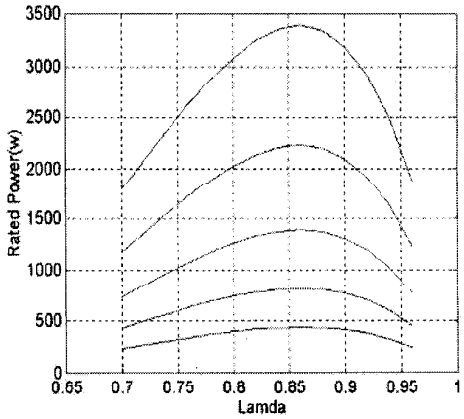

Fig. 8. The rated power vs. parameter λ for AFCC machine with different diameter. (Speed =750rpm, $D_o$ = 120, 140, 160, 180, 200 mm, from the bottom to the top)

Based on the design guidelines discussed, a prototype of an AFCC machine was designed with λ=0.78 and $K_L$=0.60. As discussed before, the selection of λ is slightly smaller than the optimal value. This is because the prototype is a relatively small machine. The electric loading corresponding to the optimal λ may be larger than that allowed by thermal conditions. On the other hand, a slightly larger $K_L$ is selected to compensate materials with poor property and extra leakage situations.

The three-dimensional finite element analysis processes are performed to facilitate the design. The results of static torque and inductance for different MMFs are shown in Fig. 10 and Fig. 11.

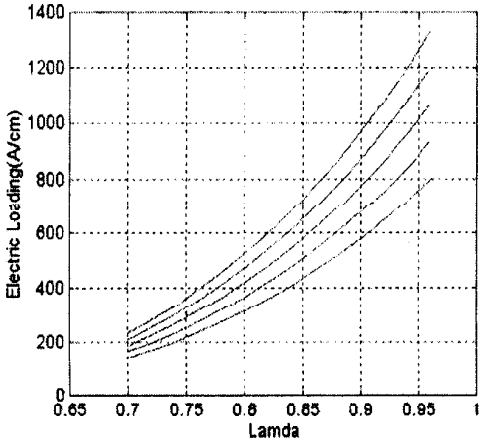


Fig. 9. The electric loading vs. parameter λ for AFCC machine with different diameter.

To verify the motor operation with a power converter, a time domain simulation is also implemented in Matlab which includes the model of the AFCC motor, power converter and control algorithms. Some of the simulation results are shown in Fig. 12.

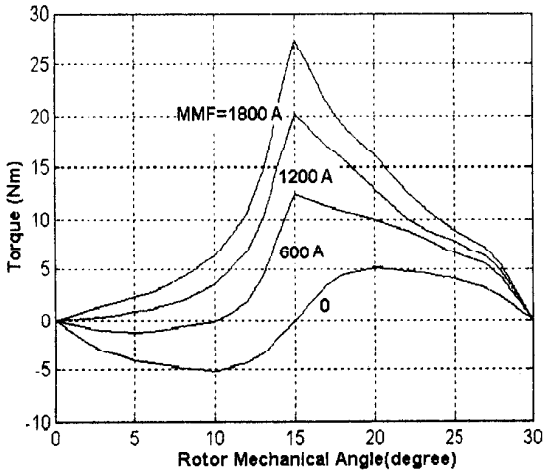


Fig. 10. Torque curves of an AFCC machine.

## IV. Manufacturing and Experimental Evaluation of the Prototype

A prototype of the single-phase 12-pole, radial airgap machine design was manufactured and the finished prototype is shown on Fig. 13.

A digital control based on Texas Instruments digital signal process is used to control the machine. The power stage consists of an H-bridge IGBT converter to provide a bipolar voltage to the machine for current control. The control algorithm is implemented as a software in the DSP. The algorithm determines the desired current profile based on the

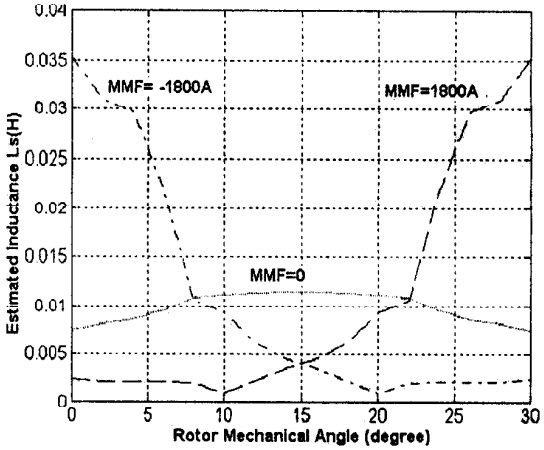


Fig. 11. The inductance of the motor.

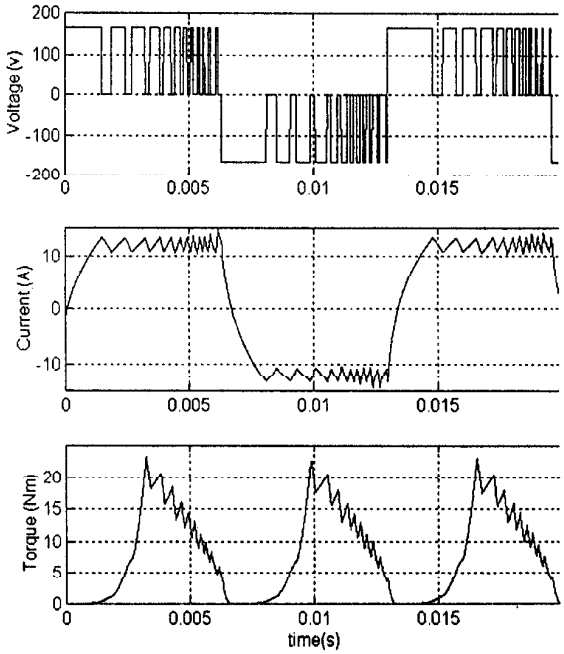


Fig. 12. Simulation results at rated speed (750 rpm) and rated current (13 A).

detected rotor position and turns on and off the switches to maintain the motor current. A PI current regulator is used to control the motor current. The algorithm is executed in less than 50μs so that the control action is updated every 50μs.

After a static test such as back emf at different speed (shown on Fig. 14), the AFCC motor was driven by a TI-DSP based controller and power inverter. The tests were conducted using a dyno with a 10 HP DC machine as the load, which is located in the Lab of Wisconsin Electric Machine and Power Electronics Consortium (WEMPEC). The voltage and current waveforms are shown on Fig. 15. The output torque is then calculated from the output of the DC motor and is shown in Fig. 16 and 17.

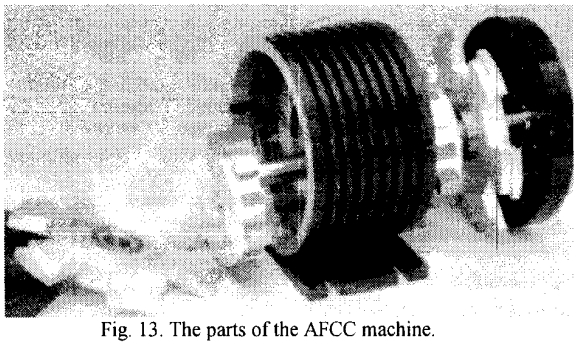

Fig. 13. The parts of the AFCC machine.

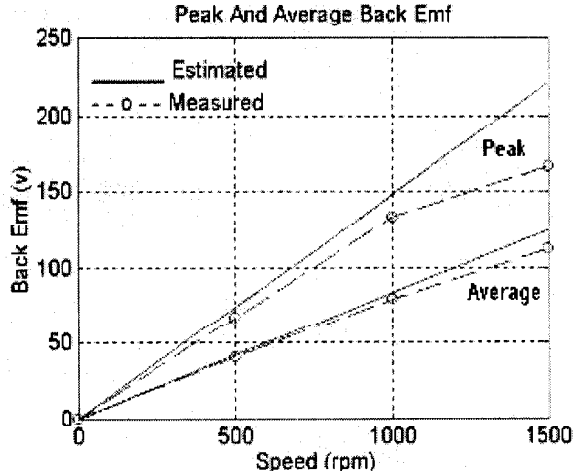


Fig. 14. The back emf at different speed.

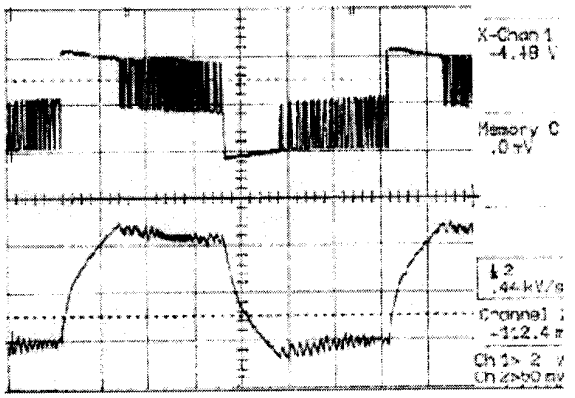

Fig. 15. The voltage and current waveform. (Speed=750rpm, Vdc=160V, Current reference=13A, Output Torque=6.38 Nm.)

In Fig. 16, the estimated torque is given by three-dimensional FEA and it is the static value. When the motor is running at low speed, for example, 250 rpm, the test result is very close the this value. However, when the motor speed increases, the difference between the estimated value and tested values becomes larger. The similar phenomena can also be observed on back emf testing (Fig. 14). This result is because the electromagnetic power passed through the airgap has to be offset by the core losses, and unfortunately the prototype is expected to have a large core loss due to the three-dimensional flux distortion over the laminated silicon iron.

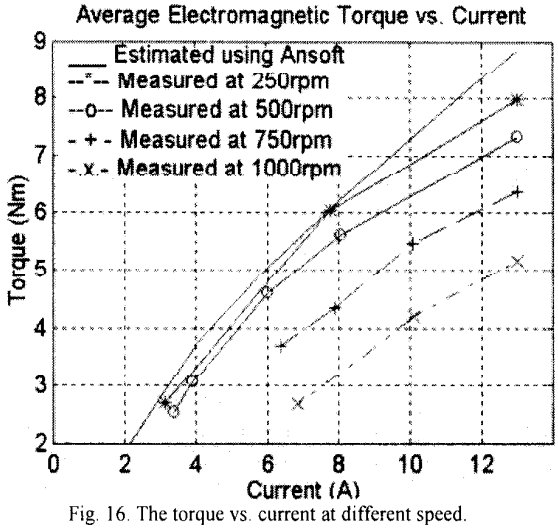


Fig. 16. The torque vs. current at different speed.

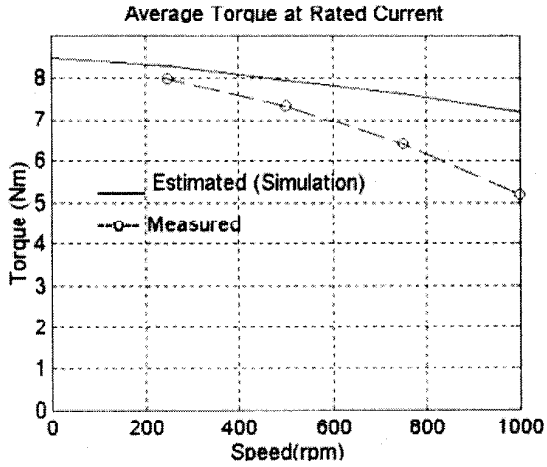


Fig. 17. Torque capability of the AFCC motor.

Provided as a reference is an estimated torque to include the rotor core losses is shown in Fig. 17. The rotor core loss is estimated based on the material loss data. The test result shows much larger rotor core losses. Although the rotor is made by silicon-iron laminations, the flux on the rotor does not follow the lamination direction perfectly. The distorted three-dimensional distributed flux causes an additional core loss. This result explains the fact that the tested result is smaller than the estimated result and the difference becomes larger as the speed increases. This feature could be a very interesting and extensive topic to estimate the core loss for that three dimensional flux distortion in laminations and further studies are being planned. Moreover, research on

using powder metal materials to reduce the core loss have also been conducted and will be discussed in future papers.

Based on the test results, the AFCC machine prototype is compared to BLDC and induction machines. Considering the difficulties to obtain data from commercial products, an alternative means is to design two BLDC machines (one with ferrite magnets and one with rare earth magnets), using commercial motor design software. The induction machine is a three-phase four-pole machine made by General Electric. The comparison is shown in Table I.

TABLE I
PERFORMANCE COMPARISON

| Parameters | AFCC | BLDC (ferrite) | BLDC (rare earth) | IM (GE) |
|---|---|---|---|---|
| Rated power (W) | 501 | 366 | 720 | 1492 |
| Rated speed (rpm) | 750 | 750 | 750 | 1725 |
| Rated torque (Nm) | 6.38 | 4.66 | 9.163 | 8.26 |
| Stator stack outer diameter (cm) | 14 | 14 | 14 | 15.875 |
| Stator stack length (cm) | 6.5 | 6.5 | 6.5 | 11.43 |
| Stator total length (including end winding) (cm) | 6.5 | 130 | 12.4 | 16.33 |
| Weight of copper (kg) | 0.5993 | 1.667 | 1.514 | |
| Cost of copper (1) (USD) | **2.10** | **5.86** | **5.32** | |
| Weight of magnet (kg) | 0.972 | 0.615 | 0.382 | |
| Cost of magnet (2) (USD) | **6.43** | **4.06** | **50.48** | |
| Motor stack volume ($cm^3$) | 1000 | 1000 | 1000 | 2262 |
| Motor total volume ($cm^3$) | 1000 | 2031 | 1909 | 3232 |
| Total circle around electric loading (A/cm) | 232 | 209 | 262 | |
| Total copper loss(W) | 58 | 131 | 88 | |
| Torque over stack volume ($Nm/cm^3$) | 0.0064 | 0.0047 | 0.0092 | 0.0037 |
| Torque Ratio : AFCC vs. other machine (stack volume) | 1 | 1.319 | 0.70 | 1.72 |
| Torque over total volume ($Nm/cm^3$) | 0.0064 | 0.0023 | 0.0048 | 0.0026 |
| **Torque Ratio : AFCC vs. other machines (total volume)** | **1** | **2.78** | **1.33** | **2.45** |

(1) Unit price of copper: 3.513 USD/kg.
(2) Unit price of magnet: Ferrite: 6.61 USD/kg; Rare earth: 132.16 USD/kg
(3) Definition for axial flux machine: Total rms current over effective length.

## V. CONLUSION

1) A modified AFCC machine topology with radial airgap is proposed. The design guidelines and parameter optimizations have been investigated by means of sizing equations and three-dimensional finite element analysis of the electromagnetic field. The results are

1. The aspect ratio $K_L$ will affect the flux concentration capability of the machine, and is also related to the pole number of the machine. For a machine with 12 poles, the optimized aspect ratio is 0.55 to 0.6. In this case, the AFCC topology will have a PM leakage factor of 0.6 to 0.64. That means 60% to 64% of the PM flux will become main flux and will be linked by the winding.
2. The optimized ratio $\lambda$ is 0.85 to 0.86. This optimized value is independent of the machine size. Although the optimized value of $\lambda$ is recommended to design the machine, other constrains such as the electric loading should also be considered based on the machine size.

2) The prototype of a single-phase 6-pole AFCC machine, as well as a closed-loop drive system based on DSP technology, has been designed, manufactured and tested. From the test results, the operating principle and torque capability of the AFCC machine have been verified and assessed. The main conclusions from the experimental investigations are as follows:

1. The prototype AFCC machine has a higher torque capability than equivalent induction machines. If comparison is based on stack volumes, the ratio is 1.72 to 1. If the comparison is based on total volumes, the ratio is 2.45 to 1. The latter is reasonably close to that estimated by sizing equations, which is 3 to 1.
2. The AFCC motor shows an obvious higher torque capability when compared to BLDC machine with ferrite magnets. The torque comparison ration is 2.78 to 1 when compared with total volume, and 1.319 to 1, when compared with the volume. The BLDC motor with rare earth magnet has higher torque capability than the AFCC motor, when compared with stack volume. However, when compare the total volume, the AFCC motor is better because it does not have end-winding portions. The torque comparison ratio is 1.33 to 1. It should be noted that the cost of rare earth magnets in BLDC motor is substantially higher compared to ferrite magnets.

ACKNOWLEDGEMENT

The authors are grateful for support from the Wisconsin Electric Machine and Power Electronics Consortium (WEMPEC) and the National Science Foundation of China (#59877014).

REFERENCES

[1] T.A. Lipo and Y. Li, "The CFM - A New Family of Electrical Machines", Conf. Rec. IPEC (Japan), April 3-7, 1995, pp. 1-8 (keynote paper).

[2] S. Huang, J. Luo, F. Leonardi, and T. A. Lipo, "A General Approach to Sizing and Power Density Equations for Comparison of Electrical Machines", IEEE -IAS Annual Meeting, Oct. 1996, San Diego, CA, pp. 836-842.

[3] A. G. Jack, B. C. Mecrow, C. P. Maddison; N. A. Wahab, "Claw pole armature permanent magnet machines exploiting soft iron powder metallurgy", 1997 IEEE International Electric Machines and Drives Conference Record, May 1997, Milwaukee,WI,v+734 pp.MA1/5.1-3.

[4] H. Weh, "On the Development of Inverter Fed Reluctance Machines for High Power Densities and High Outputs", etz Archiv, Bd. 6, 1984, pp. 135-144 (In German).

[5] S. Huang, J. Luo and T. A. Lipo, "Analysis and Evaluation of the Transverse Flux Circumferential Current Machine", IEEE-IAS Annual Conference Record. Oct. 1997. New Orleans, Louisiana, pp. 378—384.

[6] Jian Luo, Dinyu Qin, Thomas A. Lipo, Shuxiang Li, Surong Huang, "Axial Flux Circumferential Current Permanent Magnet Machine", IEEE-IAS Conference Record, Oct. 1998, St. Louis, MO, pp. 144-151.